
Article:
Taylor-Mew, J. orcid.org/0000-0002-0895-2968, Collins, X. orcid.org/0000-0003-1323-7907, White, B. orcid.org/0000-0001-8785-7151 et al. (2 more authors) (2024) Development of InGaAs/AlGaAsSb Geiger mode avalanche photodiodes. IEEE Transactions on Electron Devices, 71 (3). pp. 1994-1998. ISSN 0018-9383

https://doi.org/10.1109/ted.2024.3354698

Development of InGaAs/AlGaAsSb Geiger mode Avalanche Photodiodes

J. Taylor-Mew, X. Collins, B. White, C. H. Tan, *Senior Member, IEEE,* and J. S. Ng, *Member, IEEE*

Abstract— Near-infrared linear mode $Al_{0.85}Ga_{0.15}As_{0.56}Sb_{0.44}$ avalanche photodiodes (APDs) exhibit excellent temperature stability, potentially simplifying Geiger mode operation. We have carried out the first experimental evaluation of $In_{0.53}Ga_{0.47}As/Al_{0.85}Ga_{0.15}As_{0.56}Sb_{0.44}$ APDs in Geiger mode. Characterization on multiple devices included temperature-dependent dark current, avalanche multiplication, dark count rate, afterpulsing, and single photon detection efficiency (SPDE). The temperature coefficient of breakdown voltage extracted from avalanche multiplication data was 13.5 $mV.K^{-1}$, much lower than InGaAs/InP Geiger mode APDs, reducing changes in operation voltage and offering possible protection from high optical power thermal attack in communication systems. At 200 K, SPDE were 5-16 % with dark count rate of 1-20 $Mc.s^{-1}$, comparable to InAlAs and early InP-based Single Photon APDs. The afterpulsing at 200 K was negligible for hold-off time > 50 µs (reducing to 5 µs at 250 K). These are similar to the performance of InGaAs/InAlAs and some InGaAs/InP Geiger mode APDs. The data reported in this article is available from the ORDA digital repository (https://doi.org/10.15131/shef.data.24125721)

***Index Terms*— Single Photon Detection efficiency, AlGaAsSb, Single Photon Avalanche Photodiode, Geiger Mode Avalanche Photodiode, SPAD**

I. Introduction

Single Photon Detection is increasingly important due to rising demands for applications such as laser ranging [1], Quantum Key Distribution [2], and remote gas sensing [3]. The operation wavelength of these applications is often ~ 1550 nm, either to utilize the low-loss window in optical fiber-based systems or to better penetrate atmospheric obscurants in free-space systems. The dominant single-photon detector technologies for 1550 nm wavelength photons are Superconducting Nanowires Single Photon Detectors (SNSPDs) [4] and Single Photon Avalanche Diodes (SPADs) [5]. SPADs are Avalanche Photodiodes (APDs) operated in Geiger mode to achieve single photon detection. For both detector technologies, low Dark Count Rate (DCR) and high SPDE are two of the most important performance metrics. SNSPDs provide Single Photon Detection Efficiency (SPDE) as high as 90 % [6] but require cryogenic operation temperature (< 4 K), limiting widespread adoption. SPDE values of SPADs are much lower, at ~20 – 60 % [7], but they can be cooled using inexpensive and compact thermoelectric coolers. Hence, SPADs remain the single photon detector of choice for many applications.

The most dominant SPADs for ~ 1550 nm wavelength are InGaAs/InP SPADs, which are available commercially from several vendors (e.g. [8] and [9]). They use $In_{0.53}Ga_{0.47}As$ (lattice-matched to InP substrates), hereafter referred to as InGaAs, to absorb infrared photons and InP for avalanche breakdown [10-19]. SPADs for 1550 nm wavelength are operated beyond their breakdown voltage (V_{bd}) and often in gated mode, so DCR, i.e., the number of false counts expected for a free-running device, should be used when comparing SPADs. InGaAs/InP SPADs operated at 200 – 300 K and 1550 nm wavelength have so far resulted in combinations of DCR and SPDE of 10^2-10^5 cps and 20-40 %, respectively [7,20]. Incorporating micro-lens and Distributed Bragg Reflector could improve the SPAD's performance (e.g., 500 cps and 40 % at 223 K) [16]. Reducing temperature can reduce the DCR (e.g., 15 cps at 163 K [18]). Implementing sinusoidal gating has allowed SPADs to achieve SPDE as high as ~ 60 % at room temperature, albeit with high DCRs [13,14].

The InGaAs/InP combination for SPADs originated from the APDs for O- and C-band optical communication systems.

This work was supported by UK Research and Innovation (project 10031973) (*Corresponding author: J. S. Ng*)

J. Taylor-Mew, C. H. Tan, and J. S. Ng are with the Department of Electronic and Electrical Engineering, The University of Sheffield, Sheffield S1 3JD, U.K. (e-mail: j.taylor-mew@sheffield.ac.uk; c.h.tan@sheffield.ac.uk; j.s.ng@sheffield.ac.uk) X.Collins and B. White are with Phlux Technology Ltd., Sheffield S3 7HQ, U.K. (e-mail: xiao.collins@phluxtechnology.com; ben.white@phluxtechnology.com).

Although the avalanche material InP benefits from a mature manufacturing process, its temperature stability of avalanche characteristics, characterized by thermal coefficient of breakdown voltage, C_{bd}, is worse than alternative avalanche materials, such as $In_{0.52}Al_{0.48}As$, hereafter referred to as InAlAs [21]. Coupled with potentially higher avalanche breakdown probability, SPADs using InAlAs avalanche layers have been reported [22-27]. However, their performance is still below those of InGaAs/InP SPADs (InAlAs SPADs typically exhibit higher DCR than InP SPADs for a given SPDE). For example, the best $In_{0.52}Al_{0.48}As$ SPAD exhibits a DCR and SPDE (at 1550 nm wavelength) of 35 Mcps and ~35 % [25], inferior to the InP SPADs.

Recently, $Al_{0.85}Ga_{0.15}As_{0.56}Sb_{0.44}$ (AlGaAsSb) has emerged as a superior avalanche material for Linear mode APDs, with experimental reports of highly dissimilar ionization coefficients [28] and low excess noise factor [29] (resulting in very low Noise-Equivalent-Power [30]). Reported values of C_{bd} for a GaAsSb/AlGaAsSb SAM APD are ~4 mV/K [31], lower than equivalent InGaAs-based APDs with InP (~100 $mV.K^{-1}$) [32] and InAlAs (~20-50 $mV.K^{-1}$) [23-26] avalanche layers. Having very low C_{bd} values is advantageous for achieving SPADs with higher operation stability. This can help counteract changes in required overbias if the SPAD is flooded with high optical power thermal attack, one of the possible attack methods on optical communication systems utilizing SPADs [33]. However, there is as yet no experimental report of SPADs using $Al_{0.85}Ga_{0.15}As_{0.56}Sb_{0.44}$ avalanche layer. In this work, we report Linear and Geiger mode experimental data of an InGaAs/AlGaAsSb APD operated at 200 K and ~ 1550 nm wavelength.

II. Experimental Details

The InGaAs/AlGaAsSb APD wafer was grown on a semi-insulating InP substrate using molecular beam epitaxy. The wafers were designed and fabricated into mesa devices (using standard contact lithography and wet chemical etching) by Phlux Technology Ltd [30]. The InGaAs photon absorption layer and the AlGaAsSb avalanche layer are separated by a charge sheet to minimize the electric field and band-to-band tunneling in the InGaAs layer. The devices were characterized in both Linear mode and Geiger mode operation. The former included temperature-dependent Current-Voltage (in the dark and under 1550 nm illumination) and avalanche multiplication ($M(V)$) on devices with 230 μm diameter. The latter included temperature-dependent DCR and SPDE on devices with 50 μm diameter, since SPADs typically have smaller active areas than APDs to reduce the absolute dark currents. All measurements were performed with the device-under-test (DUT) inside a low-temperature probe station.

The forward and reverse Current-Voltage characteristics of three devices were measured using a source-measure-unit with the DUTs at 200 – 300 K. To accurately measure $M(V)$ against the dark current, a phase-sensitive detection technique was implemented using a modulated laser light (1550 nm wavelength, 50 % duty cycle, and 10 kHz repetition frequency) and a lock-in amplifier. $M(V)$ data were obtained at 200 – 300 K (using three devices for each temperature) for extraction of C_{bd}.

The DCR and SPDE measurements were carried out using the setup described in [23]. The DUT was reverse-biased in a gated mode, i.e. voltage pulses (referred to as a.c.) were superimposed onto a d.c. bias, bringing the total bias on the DUT beyond the breakdown voltage only during the voltage pulse duration. The voltage gate pulses had an amplitude of ~ 8 V, on-time (t_{on}) of 20 ns (including 5 ns rising edge and 5 ns falling edge), and a repetition rate (f) of 100 kHz unless otherwise stated. As the d.c. bias increased (always below V_{bd}), the effective overbias on the DUT increased from 0 to 8 V. A combination of a variable capacitor and a differential amplifier were added to reduce capacitive transients within the DUT's avalanche current signals [34], before being detected by an edge-triggered discriminator. The signal from the discriminator was recorded using a counter, yielding a measured count rate (C_{rate}).

When the DUT was kept in the dark, gated measurements yielded the raw dark count rate (C_{rate_dark}). The DCR was obtained from

$$\mathrm{DCR} = -\left[\ln\left(1-\frac{C_{rate\_dark}}{f}\right)\right]/t_{on}\,, \qquad (1)$$

derived from $C_{rate\_dark} = f\,[1\text{-}\exp(\text{-DCR} \times t_{on})]$ [34]. Afterpulsing was assessed by repeating gated DCR measurements at different f.

The SPDE measurements used a 1566.5 nm wavelength pulsed laser (pulse width ~ 23 ps) and a variable optical attenuator to adjust the average number of photons per pulse ($\bar{N}$) falling on the DUT ($\bar{N} = 0.1$). The pulsed laser and optical attenuator settings were confirmed through optical power measurement for each SPDE measurement session. SPDE was given by [35]

$$\mathrm{SPDE} = \frac{P_t - P_d}{1 - \exp\left(-\bar{N}\right)}\,, \qquad (2)$$

where P_t and P_d are the probability of detecting an event with and without photon(s) injection, respectively, these were obtained experimentally using C_{rate}/f. Eqn. (2) assumes only one event can be recorded in a single voltage pulse period, which is appropriate in our SPDE measurements [36]. For some of our DCR and SPDE measurements, additional data of the avalanche event's timing was recorded using a combination of a delay generator (Ortec 416A), a time-to-amplitude converter (Ortec 566), and a multichannel analyzer (Canberra Multiport II).

III. Results and Discussion

Temperature (T) dependent Current-Voltage characteristics in the dark are shown in Fig. 1(a). For a given temperature, the data from the three devices are indistinguishable hence mean values are presented. At 300 K the dark current increases rapidly at ~ 65 V, which was later confirmed as the V_{bd}. At 250 K and below, the dark current increases gradually between 50 V and V_{bd}, indicating onset of significant impact ionization (also observed in photocurrent increase with reverse bias). This is supported by the analysis of the activation energy of the dark counts presented later. As temperature decreases, V_{bd} reduces, as expected for AlGaAsSb APDs [31]. Current-Voltage characteristics of the same devices when illuminated with 1550

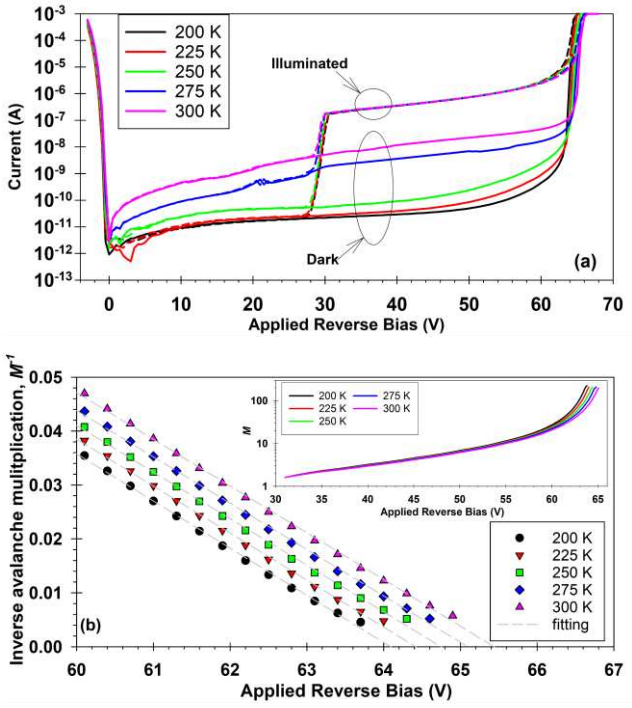

Fig. 1. (a) Reverse Current-Voltage data at 200 to 300 K, under dark (solid lines) and 1550 nm wavelength illumination (dashed lines). (b) $M^{-1}(V)$ data and linear regression fittings. $M(V)$ are shown in inset of (b). All data were mean values from three devices (230 μm diameter).

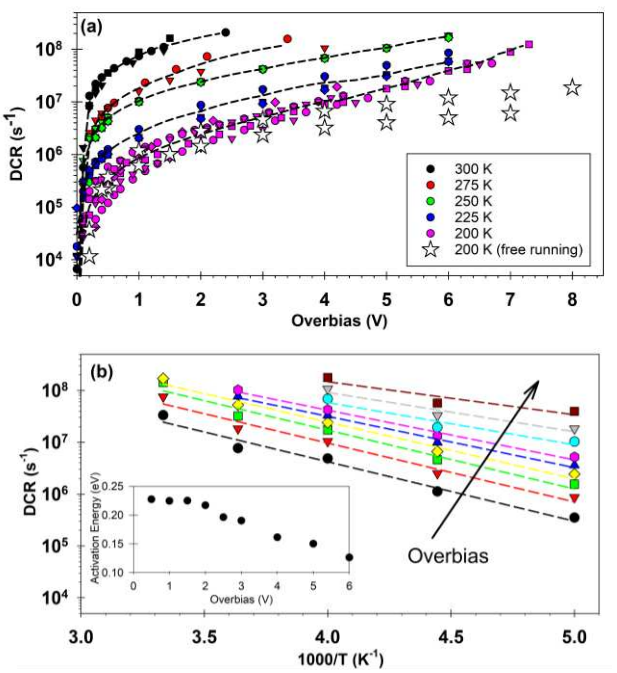

Fig. 2. (a) Normalized DCR data (symbols) and mean values (dashed lines) versus overbias at 200 to 300 K from gated and free running measurements. (b) Normalized DCR versus 1000/T (symbols) and fittings (dashed lines) at 0.5, 1.0, 1.5, 2.0, 2.5, 3.0, 4.0, 5.0, and 6.0 V overbias (from bottom to top). (Inset) activation energy versus overbias. Data were obtained from 50 μm diameter devices.

nm wavelength light are also shown in Fig. 1(a). A sudden increase in photocurrent occurred ~ 31 V, indicating punch-through (i.e. the depletion region has reached the InGaAs absorption layer).

The avalanche multiplication data (from three devices) for T = 200 to 300 K are shown in Fig. 1(b)(inset). The data assumed that M at punch-through for our APD was ~ 1.62, given by the ratio of our APD's responsivity (1.45 A.W^{-1}) to the responsivity of a reference InGaAs/AlGaAsSb APD with a unity gain at the punchthrough voltage (~0.90 A.W^{-1}). The largest value of M obtained reliably was ~ 200. The mean $M^{-1}(V)$ data are plotted against T in Fig. 1(b). Values of breakdown voltage were extracted by extrapolating $M^{-1}(V)$ to zero for each temperature point, yielding a C_{bd} value of 13.5 mV.K^{-1}. This is much lower compared to ~100 mV.K^{-1} [32] and 20-50 mV.K^{-1} [23-26] for InGaAs/InP and InGaAs/InAlAs APDs.

DCR versus overbias data at 200, 225, 250, 275, and 300 K are shown in Fig. 2(a). For a given overbias, the DCR decreases as temperature decreases, with ~ 2 orders of magnitude reduction from 300 to 200 K. The DCR at 200 K is supported by an additional 200 K DCR data from free-running operation (using a 360 kΩ ballast resistor for passive quenching), also shown in Fig. 2(a). They are in agreement between 0 and 5 V overbias, after which ineffective quenching of the avalanche pulses in free-running operation limits the maximum DUT avalanche counts.

Plotting the DCR versus 1000/T as a function of overbias, as shown in Fig. 2(b), facilitated the extraction of the activation energy (E_a) of the DCR using DCR ∝ exp[-E_a/(kT)], where k is the Boltzmann constant. The corresponding E_a values obtained are 0.23 to 0.13 eV for ΔV of 0.5 to 6.0 V. The largest E_a value (0.23 eV) is less than 0.38 eV (half of $In_{0.53}Ga_{0.47}As$ bandgap) and E_a decreases with overbias. The likely cause of the dark counts observed is therefore generation-recombination and tunneling (which has a weak temperature dependence) in the APD or a combination of them [23,37]. Since avalanche breakdown dominates band-to-band tunneling current in AlGaAsSb avalanche regions [38], the source of tunneling currents is likely to be the narrow bandgap InGaAs absorber.

The number of dark counts versus time from a device (obtained using the delay generator, time-to-amplitude converter, and multichannel analyzer) at 200 K and overbias of 1 to 5 V are shown in Fig. 3(a). As the overbias increases, the recorded dark counts occur within a longer time window. This is because the portion of the a.c. voltage pulse above the V_{bd} increases with the d.c. bias (with a fixed a.c. voltage amplitude), as illustrated in Fig. 3(a)(inset). The data confirm that well-behaved a.c. voltage pulses appeared across the DUT as intended during the gated Geiger mode measurements. Also, the uniform distribution of dark counts versus time indicates that the dark counts originated primarily from bulk dark carriers rather than trapped carriers. The increase in counts at the rising edge for 5 V overbias is attributed to the increase in afterpulsing (as shown later in Fig. 5). We ruled out contributions from capacitive transients since the a.c. voltage amplitude remains constant in these measurements.

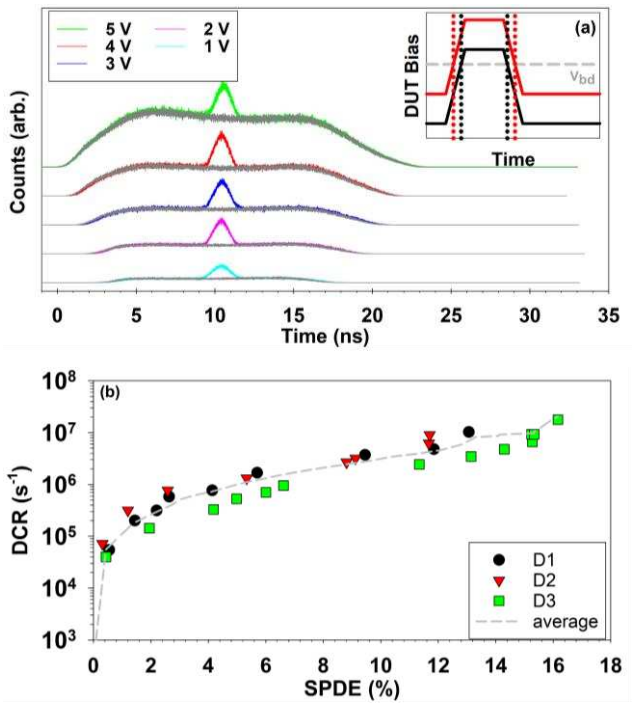

Fig. 3. (a) Counts of avalanche events versus time from DCR (grey) or SPDE measurements (color) at 200 K as a function of overbias. Data from different overbias voltages offset vertically for clarity. (b) DCR versus SPDE data for three 50 μm diameter devices (symbols) and their mean values (line) at 200 K.

The measurements were repeated with an injection of 0.1 photon per pulse. The data (also shown in Fig. 3(a)) are similar to the dark count data, but there are now peaks generated by photon injection. Before and after the photon peak, the number of counts is indistinguishable from those of dark count. From these data, we extracted the values for P_t and P_d to calculate SPDE (for three devices) at 200 K. The SPDE values are plotted against DCR in Fig. 3(b). The highest SPDE of ~16 %, with a DCR ~ 20 Mcps, occurred at 5 V overbias. At higher bias, the SPDE started to fall due to high dark counts preventing the detection of signal photons. The InGaAs/AlGaAsSb APDs exhibited increasing SPDE at the expense of increasing DCR. The photon peak duration is dominated by the timing uncertainty of the measurement equipment (~1 ns).

DCR (scaled to device area) versus SPDE data of our InGaAs/AlGaAsSb APDs are compared with reported values

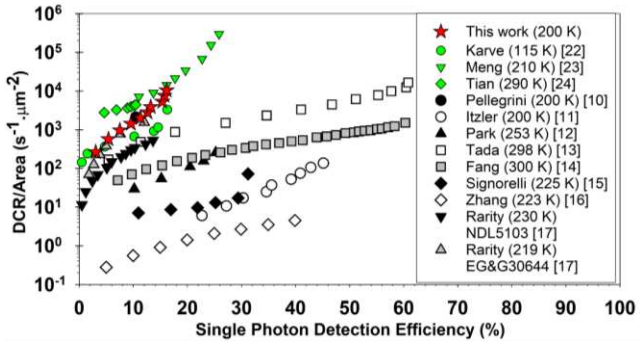

Fig. 4 DCR versus SPDE data from this work (star) and reports using InAlAs [22-24] (green) and InP [10-17] (black/white/grey) avalanche layers.

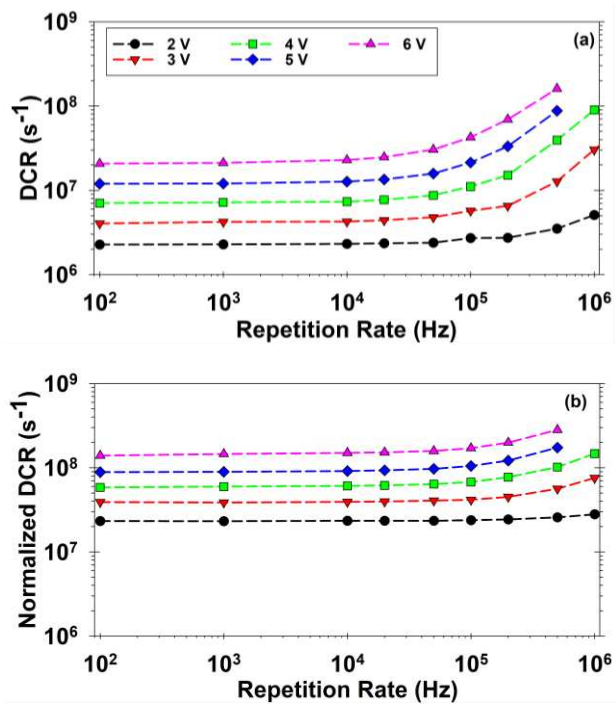

Fig. 5. Mean DCR versus repetition rate characteristics for three 50 μm diameter devices at 200 K (a) and 250 K (b) .

for InP [10-17] and InAlAs [22-24] SPADs in Fig. 4. Scaling to device area was necessary because of different device areas used in the various reports. Although this work does not yet match the best SPDE or lowest DCR of the state-of-the-art InGaAs/InP SPADs, the performance of our InGaAs/AlGaAsSb APDs is similar to those of InAlAs SPADs and older InGaAs/InP SPADs [10,17] for both DCR and SPDE. It is encouraging despite the AlGaAsSb APDs originally designed for linear mode operation and having relatively large device areas. Adapting the wafer design for operation beyond the breakdown voltage, optimization in wafer growth, fabrication, and reducing the device areas are expected to produce InGaAs/AlGaAsSb SPADs with lower DCRs than those of this work.

The extent of afterpulsing, an important aspect of 1550 nm wavelength SPADs, in the AlGaAsSb APDs, is evaluated in Fig. 5. The DCR were measured as functions of f and overbias at 200 K, with a fixed a.c. voltage pulse duration (20 ns). At 1 V overbias, the DCR does not vary with f. For all other overbias, as f increases (and hold-off time decreases), the DCR remains constant but starts to increase with f eventually. The inflection point occurs at a lower frequency for data obtained at higher overbias. At 6 V overbias and 200 K, the DCR increases with f when $f \geq$ 20 kHz, corresponds to a hold-off time of 50 μs. Similar data obtained at 250 K exhibit the same trends, but the inflection points occur at higher frequencies (e.g. 200 kHz for 6 V overbias). These characteristics are in line with or better than those of InGaAs/InP SPADs and InGaAs/InAlAs SPADs [10, 11, 15].

IV. Conclusion

We have characterized an $In_{0.53}Ga_{0.47}As/Al_{0.85}Ga_{0.15}As_{0.56}Sb_{0.44}$ APD originally designed for Linear mode operation in both Linear and Geiger modes. In Linear mode, the APD achieved M ~ 200 at room temperature when illuminated by a 1550 nm wavelength light. The thermal coefficient of the APD breakdown voltage was found to be 13.5 $mV.K^{-1}$, much lower than the values of InAlAs and InP SPADs. In Geiger Mode, at 200 K and standard gated mode operation, the APD achieved a maximum SPDE of ~16 % with a DCR ~20 Mcps, competitive with InAlAs SPADs. Analyses of the temperature dependence of DCR data indicated generation-recombination current and tunneling are possible contributors to dark count rates at all overbias. Hence, there is potential to improve the performance of InGaAs/AlGaAsSb SPADs through improved wafer design and reduced device area.

References

1. S. K. Poultney, 'Single Photon Detection and Timing in the Lunar Laser Ranging Experiment', IEEE Trans. Nucl. Sci., vol. 19, no. 3, pp. 12–17, Jun. 1972, doi: 10.1109/TNS.1972.4326697.
2. N. Gisin, G. Ribordy, W. Tittel, and H. Zbinden, 'Quantum cryptography', Rev. Mod. Phys., vol. 74, no. 1, p. 145, 2002, doi: 10.1103/RevModPhys.74.145.
3. J. Titchener, D. Millington-Smith, C. Goldsack, G. Harrison, A. Dunning, X. Ai, M. Reed, 'Single photon Lidar gas imagers for practical and widespread continuous methane monitoring', Appl. Energy, vol. 306, p. 118086, Jan. 2022, doi: 10.1016/j.apenergy.2021.118086.
4. D. V. Morozov, A. Casaburi, and R. H. Hadfield, 'Superconducting photon detectors', Contemp. Phys., vol. 62, no. 2, pp. 69–91, Apr. 2021, doi: 10.1080/00107514.2022.2043596.
5. J. Zhang, M. A. Itzler, H. Zbinden, and J. -W. Pan, 'Advances in InGaAs/InP single-photon detector systems for quantum communication', Light Sci. Appl., vol. 4, no. 5, pp. e286–e286, May 2015, doi: 10.1038/lsa.2015.59.
6. F. Marsili, V. B. Verma, J. A. Stern, S. Harrington, A. E. Lita, T. Gerrits, I. Vayshenker, B. Baek, M. D. Shaw, R. P. Mirin, S. W. Nam, 'Detecting single infrared photons with 93% system efficiency', Nat. Photonics, vol. 7, no. 3, pp. 210–214, Mar. 2013, doi: 10.1038/nphoton.2013.13.
7. R. Hadfield, J. Leach, F. Fleming, D. J. Paul, C. H. Tan, J. S. Ng, R. K. Henderson, G. S. Buller, 'Single-Photon Detection for Long-Range Depth Imaging', Optica, Jul. 2023, doi: 10.1364/OPTICA.488853.
8. Micro Photon Devices, 'PDM-IR'. http://www.micro-photon-devices.com/Products/Photon-Counters/PDM-IR (accessed Oct. 24, 2022).
9. Wooriro, 'Negative Feedback Avalanche Diode'. http://www.wooriro.com/en/bbs/board.php?bo_table=product04&wr_id=4 (accessed Jun. 21, 2023).
10. S. Pellegrini, R. E. Warburton, L. J. J. Tan, J. S. Ng, A. B. Krysa, K. Groom, J. P. R. David, S. Cova, M. J. Robertson, G. S. Buller, 'Design and Performance of an InGaAs–InP Single-Photon Avalanche Diode Detector', IEEE J. Quantum Electron., vol. 42, no. 4, pp. 397–403, Apr. 2006, doi: 10.1109/JQE.2006.871067.
11. M. A. Itzler, R. Ben-Michael, C. -F. Hsu, K. Slomkowski, A. Tosi, S. Cova, F. Zappa, R. Ispasoiu , 'Single photon avalanche diodes (SPADs) for 1.5 μm photon counting applications', J. Mod. Opt., vol. 54, no. 2–3, pp. 283–304, Jan. 2007, doi: 10.1080/09500340600792291.
12. C. Park, S.-B. Cho, C.-Y. Park, S. Baek, and S.-K. Han, 'Dual anode single-photon avalanche diode for high-speed and low-noise Geiger-mode operation', Opt. Express, vol. 27, no. 13, p. 18201, Jun. 2019, doi: 10.1364/OE.27.018201.
13. A. Tada, N. Namekata, and S. Inoue, 'Saturated detection efficiency of single-photon detector based on an InGaAs/InP single-photon avalanche diode gated with a large-amplitude sinusoidal voltage', Jpn. J. Appl. Phys., vol. 59, no. 7, p. 072004, Jul. 2020, doi: 10.35848/1347-4065/ab9625.
14. Y.-Q. Fang, W. Chen, T.-H, Ao, C. Liu, X.-J Gao, J. Zhang, J.-W. Pan, 'InGaAs/InP single-photon detectors with 60% detection efficiency at 1550 nm', Rev. Sci. Instrum., vol. 91, no. 8, p. 083102, Aug. 2020, doi: 10.1063/5.0014123.
15. F. Signorelli, F. Telesca, E. Conca, A. D. Frera, A. Ruggeri, A. Giudice, A. Tosi, 'Low-Noise InGaAs/InP Single-Photon Avalanche Diodes for Fiber-Based and Free-Space Applications', IEEE J. Sel. Top. Quantum Electron., vol. 28, no. 2: Optical Detectors, pp. 1–10, Mar. 2022, doi: 10.1109/JSTQE.2021.3104962.
16. B. Zhang, S. Yin, Y. Liu, Z. Jiang, W. He, Q. Li, J. Hao, L. Wang, 'High Performance InGaAs/InP Single-Photon Avalanche Diode Using DBR-Metal Reflector and Backside Micro-Lens', J. Light. Technol., vol. 40, no. 12, pp. 3832–3838, Jun. 2022, doi: 10.1109/JLT.2022.3153455.
17. J. G. Rarity, T. E. Wall, K. D. Ridley, P. C. M. Owens, and P. R. Tapster, 'Single-photon counting for the 1300–1600-nm range by use of Peltier-cooled and passively quenched InGaAs avalanche photodiodes', Appl. Opt., vol. 39, no. 36, p. 6746, Dec. 2000, doi: 10.1364/AO.39.006746.
18. B. Korzh, N. Walenta, T. Lunghi, N. Gisin, and H. Zbinden, 'Free-running InGaAs single photon detector with 1 dark count per second at 10% efficiency', Appl. Phys. Lett., vol. 104, no. 8, p. 081108, Feb. 2014, doi: 10.1063/1.4866582.
19. E. Kizilkan, U. Karaca, V. Pešić, M.-J. Lee, C. Bruschini, A. J. SpringThorpe A. W. Walker, C. Flueraru, O. J. Pitts, E. Charbon, 'Guard-Ring-Free InGaAs/InP Single-Photon Avalanche Diode Based on a Novel One-Step Zn-Diffusion Technique', IEEE J. Sel. Top. Quantum Electron., vol. 28, no. 5: Lidars and Photonic Radars, pp. 1–9, Sep. 2022, doi: 10.1109/JSTQE.2022.3162527.
20. C. Liu, H.-F. Ye, and Y.-L. Shi, 'Advances in near-infrared avalanche diode single-photon detectors', Chip, vol. 1, no. 1, p. 100005, Mar. 2022, doi: 10.1016/j.chip.2022.100005.
21. L. J. J. Tan, D. S. G. Ong, J. S. Ng, C. H. Tan, S. K. Jones, Y. Qian, J. P. R. David, 'Temperature Dependence of Avalanche Breakdown in InP and InAlAs', IEEE J. Quantum Electron., vol. 46, no. 8, pp. 1153–1157, Aug. 2010, doi: 10.1109/JQE.2010.2044370.
22. G. Karve, X. Zhang, X. Li, N. Li, S. Wang, F. Ma, A. Holmes, J. Campbell, G. S. Kinsey, J. C. Boisvert, T. D. Isshiki, R. Sudharsanan, D. S. Bethune, W. P. Risk, 'Geiger mode operation of an $In_{0.53}Ga_{0.47}As$-$In_{0.52}Al_{0.48}As$ avalanche photodiode', IEEE J. Quantum Electron., vol. 39, no. 10, pp. 1281–1286, Oct. 2003, doi: 10.1109/JQE.2003.817244.
23. X. Meng, S. Xie, X. Zhou, N. Calandri, M. Sanzaro, A. Tosi, C. H. Tan, J. S. Ng, 'InGaAs/InAlAs single photon avalanche diode for 1550 nm photons', R. Soc. Open Sci., vol. 3, no. 3, p. 150584, Mar. 2016, doi: 10.1098/rsos.150584.
24. Y. Tian, Q. Li, W. Ding, D. Wu, Z. Lin, X. Feng, G. Zhang, X. Yu, Y. Zhao, 'High Speed and High Sensitivity InGaAs/InAlAs Single Photon Avalanche Diodes for Photon Counting Communication', J. Light. Technol., vol. 40, no. 15, pp. 5245–5253, Aug. 2022, doi: 10.1109/JLT.2022.3174962.
25. J. Zhang, H. Wang, G. Zhang, K. H. Tan, S. Wicaksono, H. Xu, C. Wang, Y. Chen, Y. Liang, C. C. W. Lim, S. -F, Yoon, X. Gong, 'High-performance InGaAs/InAlAs single-photon avalanche diode with a triple-mesa structure for near-infrared photon detection', Opt. Lett., vol. 46, no. 11, p. 2670, Jun. 2021, doi: 10.1364/OL.424606.
26. Y.-S. Lee, Y. -M. Liao, P. -Li. Wu, C. -E. Chen, Y. -J. Teng, Y. -Y. Hung, J. -W. Shi, '$In_{0.52}Al_{0.48}As$ Based Single Photon Avalanche Diodes With Stepped E-Field in Multiplication Layers and High Efficiency Beyond 60%', IEEE J. Sel. Top. Quantum Electron., vol. 28, no. 2: Optical Detectors, pp. 1–7, Mar. 2022, doi: 10.1109/JSTQE.2021.3114130.
27. S.-L. Wu, Naseem, J. -M. Wun, R. -L. Chao, J. J. -S. Huang, N. -W. Wang, Y. -H. Jan, H. -S. Chen, C. -J. Ni, H. -S. Chang, E. Chou, J. -W. Shi, 'High-Speed $In_{0.52}Al_{0.48}As$ Based Avalanche Photodiode With Top-Illuminated Design for 100 Gb/s ER-4 System', J. Light. Technol., vol. 36, no. 23, pp. 5505–5510, Dec. 2018, doi: 10.1109/JLT.2018.2876168.
28. J. D. Taylor-Mew, J. D. Petticrew, C. H. Tan, and J. S. Ng, 'Simulation of $Al_{0.85}Ga_{0.15}As_{0.56}Sb_{0.44}$ avalanche photodiodes', Opt. Express, vol. 30, no. 11, p. 17946, May 2022, doi: 10.1364/OE.458922.
29. J. Taylor-Mew, V. Shulyak, B. White, C. H. Tan, and J. S. Ng, 'Low Excess Noise of $Al_{0.85}Ga_{0.15}As_{0.56}Sb_{0.44}$Avalanche Photodiode From Pure Electron Injection', IEEE Photonics Technol. Lett., vol. 33, no. 20, pp. 1155–1158, Oct. 2021, doi: 10.1109/LPT.2021.3110123.
30. X. Collins, B. Sheridan, D. Price, Y. Cao, T. Blain, J. S. Ng, C. H. Tan, B. White, 'Low-noise AlGaAsSb avalanche photodiodes for 1550 nm light detection', in Optical Components and Materials XX, M. J. Digonnet and S. Jiang, Eds., San Francisco, United States: SPIE, Mar. 2023, p. 24. doi: 10.1117/12.2651669.
31. Y. Cao, T. Osman, E. Clarke, P. K. Patil, J. S. Ng, and C. H. Tan, 'A GaAsSb/AlGaAsSb Avalanche Photodiode with a very small

Temperature Coefficient of Breakdown Voltage', J. Light. Technol., pp. 1–1, 2022, doi: 10.1109/JLT.2022.3167268.

32. T. He, X. Yang, Y. Tang, R. Wang, and Y. Liu, 'High photon detection efficiency InGaAs/InP single photon avalanche diode at 250 K', J. Semicond., vol. 43, no. 10, p. 102301, Oct. 2022, doi: 10.1088/1674-4926/43/10/102301.
33. L. Lydersen, C. Wiechers, C. Wittmann, D. Elser, J. Skaar, and V. Makarov, 'Thermal blinding of gated detectors in quantum cryptography', Opt. Express, vol. 18, no. 26, p. 27938, Dec. 2010, doi: 10.1364/OE.18.027938.
34. S. J. Dimler, J. S. Ng, R. C. Tozer, G. J. Rees, and J. P. R. David, 'Capacitive Quenching Measurement Circuit for Geiger-Mode Avalanche Photodiodes', IEEE J. Sel. Top. Quantum Electron., vol. 13, no. 4, pp. 919–925, Jul. 2007, doi: 10.1109/JSTQE.2007.903595.
35. Y. Kang, H. X. Lu, Y.-H. Lo, D. S. Bethune, and W. P. Risk, 'Dark count probability and quantum efficiency of avalanche photodiodes for single-photon detection', Appl. Phys. Lett., vol. 83, no. 14, pp. 2955–2957, Oct. 2003, doi: 10.1063/1.1616666.
36. J. D. Petticrew, 'Design and Device fabrication of Silicon Single Photon Avalanche Diodes', PhD Thesis, The University of Sheffield, Department of Electronic and Electrical Engineering, 2020. [Online]. Available: uk.bl.ethos.815542
37. J. D. Taylor-Mew, 'Characterisation and Simulation of Linear and Geiger mode Avalanche Photodiodes', PhD Thesis, The University of Sheffield, Department of Electronic and Electrical Engineering, 2022.
38. G. Karve, X. Zhang, X. Li, N. Li, S. Wang, A. Holmes, J. C. Campbell, G. S. Kinsey, J. C. Boisvert, T. D. Isshiki, R. Sudharsanan, D. S. Bethune, W. P. Risk, 'Origin of dark counts in $In_{0.53}Ga_{0.47}As$ / $In_{0.52}Al_{0.48}As$ avalanche photodiodes operated in Geiger mode', Appl. Phys. Lett., vol. 86, no. 6, p. 063505, Feb. 2005, doi: 10.1063/1.1861498.